Investigation of Ethyl Peroxy Radical Conformers via Cavity Ringdown Spectroscopy of the $\tilde{A}$-$\tilde{X}$ Electronic Transition

Patrick Rupper,[†] Erin N. Sharp,[†] György Tarczay,[‡] and Terry A. Miller*,[†]

Laser Spectroscopy Facility, Department of Chemistry, The Ohio State University, 120 West 18th Avenue, Columbus, Ohio 43210, and Laboratory of Molecular Spectroscopy, Institute of Chemistry, Eötvös University, P.O. Box 32, H-1518, Budapest 112, Hungary

Received: October 2, 2006; In Final Form: November 9, 2006

Both stable conformers, trans (T) and gauche (G), of the ethyl peroxy radical and its perdeutero analogue have been observed via cavity ringdown spectroscopy (CRDS) of the $\tilde{A}^2A'$-$\tilde{X}^2A''$ electronic transition in the near-IR. Assignments of specific spectral lines to the electronic transition origin (T_{00}), to observed vibrational hot bands, and to the COO bend and the O−O stretch vibrations are given with the help of equation of motion (EOMIP) quantum chemical calculations. In particular, spectral information for the previously unknown/unassigned T conformer of ethyl peroxy is given in this study for the first time and compared to the data for the previously observed G conformer. The conformer assignment is confirmed by an analysis of the partially resolved rotational structures. The electronic origins for the T and G conformers of $C_2H_5O_2$ are located at 7362(1) and 7592(1) cm^{-1}, respectively.

1. Introduction

The oxidation of hydrocarbons is a critically important process that affects both the efficiency of our automobiles and the quality of our atmosphere. These hydrocarbons are key components in fossil fuels that serve as our chief energy source, and so their reaction with oxygen, which will inevitably occur both in combustion and atmospheric conditions, should be well understood.

Common fuels, which are typically comprised of large hydrocarbon components like *n*-heptane and isooctane, produce numerous reactive intermediates upon combustion before going to completion. One of the key intermediate products is the alkyl peroxy radicals ($RO_2^•$) at temperatures below 1000 K. The fuel compounds (RH) are oxidized primarily by an initial H-abstraction reaction with OH to produce an alkyl radical ($R^•$) that subsequently combines with O_2 to form the peroxy radical.[1] The equilibrium formation of the alkyl peroxy radical via this reaction has an effect on the overall rate of combustion and can lead to a negative temperature dependence, as has been observed at temperatures between 550 and 700 K.[2] The competition between the alkyl radical reaction with O_2 to form peroxy radicals and the alkyl radical self-reaction may be important to the amount of soot produced[3] and a complete knowledge of the chemical and physical properties of alkyl peroxy radicals, coupled with corresponding spectral diagnostics, should benefit greatly our understanding of combustion chemistry.

Peroxy radicals involved in hydrocarbon oxidation are also important to the chemistry of the troposphere[4,5] because they play a key role in the degradation of volatile organic compounds injected into the atmosphere. In the clean atmosphere, organic peroxy radicals undergo self-reactions, cross-reactions, or reactions with HO_2 to generate alcohols, carbonyl compounds, and hydroperoxides,[6] which can be involved themselves in a variety of important atmospheric processes and may also contribute to acid rain formation. In polluted atmospheres, peroxy radicals react with NO to form NO_2, which is then photolyzed to produce oxygen atoms that combine with O_2 to produce ozone. It has been estimated that the reactions of peroxy radicals are responsible for ∼90% of the ozone present in the troposphere.[7]

Because the $\tilde{B}$ state of the peroxy radicals is dissociative,[8] the well-known, strong $\tilde{B}^2A''$-$\tilde{X}^2A''$ electronic transition lying in the UV leads to a broad, structureless absorption spectrum, being only weakly dependent on the R group of the organic peroxy. To distinguish among various $RO_2^•$ radicals and also to resolve isomer and conformer structure, our group has undertaken efforts in the past to apply cavity ringdown spectroscopy (CRDS) to the $\tilde{A}^2A'$-$\tilde{X}^2A''$ electronic transition in the near-infrared (NIR).[9−15] Because this is a bound−bound transition with well-defined structure, we have been able to distinguish not only among different chemical species RO_2 and $R'O_2$ but also among different isomers and even conformers of a given RO_2 radical. For peroxy radicals with R being a simple alkyl group, we have previously reported spectra for the series from methyl peroxy ($R = CH_3$)[9] up to butyl peroxy ($R = C_4H_9$).[14] An upcoming paper[16] will present results for all the isomers of pentyl peroxy and also will summarize the characteristics and properties of all these alkyl peroxy radicals.

In this article, we report a detailed investigation of the NIR CRDS spectra of ethyl peroxy and its perdeutero analogue. The $\tilde{A}^2A'$-$\tilde{X}^2A''$ electronic near-IR transition of ethyl peroxy was first observed via absorption spectroscopy by Hunziker and Wendt[17] and later with higher resolution by our group.[9] Atkinson and Spillman[18] used this near-IR transition to study ethyl peroxy radical kinetics via cw-CRDS, whereas Nickolaisen and coworkers[19] determined experimental vibrational frequencies of ethyl peroxy in the mid-IR. However, in all the experimental studies up to now, the spectrum of only one conformer of ethyl peroxy has been reported, although calculations indicate an

* Address correspondence to this author. Phone: (614) 292-2569. Fax: (614) 292-1948. E-mail: tamiller@chemistry.ohio-state.edu.
[†] The Ohio State University.
[‡] Eötvös University.

10.1021/jp066464m CCC: $37.00
Published on Web 01/11/2007

energy separation between the two conformers of less than *kT* at room temperature.[20] It is important to understand the spectroscopy of both conformers of the penultimate smallest alkyl peroxy radical in detail to be able to understand the larger alkyl peroxy radicals, where the number of isomers and conformers dramatically increases.

2. Experimental Section

The apparatus was similar to that used in previous studies of the $\tilde{A}$-$\tilde{X}$ CRDS spectroscopy of alkyl peroxy radicals.[12,14] The required NIR radiation around 1.3 μm was generated by stimulated Raman shifting of the output of a dye laser in molecular hydrogen. The second harmonic of a Nd:YAG laser (20 Hz Quanta Ray PRO 270, Spectra Physics) pumped a dye laser (Sirah), whereby the dyes DCM, Rh B, and Rh 101 were used to cover the 588−645 nm region with pulse energies of 50−100 mJ and a laser line width of 0.03 cm^{-1} (fwhm). The output of the dye laser was focused by a 50 cm focal length lens into a 70 cm long, single-pass Raman cell filled with 200−300 psi of H_2. The required NIR light corresponds to the second Stokes radiation (1−2 mJ/pulse) in the region of 1.15−1.39 μm, and the simultaneously produced first Stokes and anti-Stokes as well as fundamental radiation were filtered out by using several 1000 nm long-pass cutoff filters. The NIR light then entered the 55 cm long ringdown cell formed by two highly reflective ($R \geq 99.99\%$) mirrors (Los Gatos Research). To cover the NIR range from 1.15 to 1.39 μm for the experiments in this work here, two sets of mirrors were used, whereby each mirror set had sufficient overlap to allow complete wavelength coverage. A constant flow of nitrogen purged the exposed surface of the mirrors to protect them from any harsh chemicals present in the cell. The NIR radiation that passed through both highly reflective mirrors and exited the ringdown cell was focused by a 2.5 cm focal length lens onto an amplified InGaAs photodiode detector, whose signal was digitized by a 12 bit 20 MHz digitizing card installed in the PC controlling the experiment. Typically 20 consecutive laser shots were averaged at each dye laser frequency and the digitized signal of the observed decay of radiation was then fit to a single-exponential by using the nonlinear Levenberg−Marquardt algorithm. The decay constant was converted to the relative absorption per pass (in ppm) and saved as a data point in the spectrum. To remove background structures, i.e., broad bands of precursor absorption and sharp rotationally resolved water lines, at each frequency point, a ringdown time was acquired with the photolysis excimer laser on and off and these two traces were subtracted (excimer on − excimer off) to leave only the spectrum due to the transient species. Frequency calibration was achieved from residual water absorption with use of the HITRAN 2004 database.[21]

To initiate the chemistry producing $C_2H_5O_2$ radicals, a photolysis ArF excimer laser (LPX 120i, Lambda Physik) at 193 nm, with pulse energies of 150 mJ, was focused by a cylindrical and a spherical lens to a rectangular shape of 0.5 × 13 cm and sent into the central part of the flow cell through the side via a UV-grade quartz window. The flux of excimer radiation passing through the ringdown cell was 1.5×10^{16} photons/cm^2. The photolysis pulse was fired 100 μs before each shot of NIR light entered the cavity, allowing time for ethyl peroxy radicals to be formed, but not enough time for them to recombine. By changing the delay time between the photolysis and excitation lasers we have the ability to investigate the reaction chemistry and kinetics of peroxy radicals.[12,14]

To produce the ethyl peroxy radicals, two different methods were applied. In the direct photolysis method, the precursor 3-pentanone was used because ethyl radicals are easily produced from it at 193 nm due to the strong absorption cross section of $\sigma \approx 2.8 \times 10^{-18}$ cm^2 /molecule.[22] Another precursor taken for this direct photolysis method was ethyl bromide. Although resulting in similar results, the spectra recorded with ethyl bromide were of lower quality due to the smaller photolysis cross section of this precursor ($\sigma \approx 7 \times 10^{-19}$ cm^2/molecule).[23] In a second ethyl peroxy production method, oxalyl chloride, $(COCl)_2$, was used to produce chlorine atoms for hydrogen abstraction from ethane resulting in ethyl radicals. Because of the large absorption cross section of oxalyl chloride ($\sigma_{OxCl} = 3.8 \times 10^{-18}$ cm^2/molecule at 193 nm),[24] this indirect approach resulted in spectra as good or better than the ones from the direct photolysis method with 3-pentanone as the precursor, and represents therefore an alternative source of ethyl radical to support spectroscopic assignments of the spectral carrier. Moreover, by having two good production methods one can choose the one suffering less from broad precursor absorption, which, although suppressed by our background subtraction procedure, nevertheless increases the baseline of the spectra and influences their S/N ratios.

In both production methods, the ethyl radicals subsequently reacted with O_2 to produce ethyl peroxy in a quantitative conversion via a 3-body collision involving N_2. Typical concentrations of reactants used for the direct photolysis method of ethyl peroxy production have been 2−3 Torr of 3-pentanone (nitrogen thereby bubbled through the liquid precursor), 50 Torr of O_2, and 125 Torr of N_2. Assuming a yield of two ethyl radicals per photon absorbed, the absorption cross section for 3-pentanone mentioned above (2.8×10^{-18} cm^2/molecule), and the estimated 1.5×10^{16} photons/cm^2 flux of 193 nm photons, the number of C_2H_5 radicals produced can readily be calculated to be 2.7×10^{15} molecules/cm^3 per Torr of 3-pentanone.

Typical concentrations of reactants used for the hydrogen abstraction method of ethyl peroxy radical generation included 0.5−1 Torr of $(COCl)_2$, 4 Torr of C_2H_6, 80 Torr of O_2, and 150 Torr of N_2. With the same photolysis flux as above and a yield of two chlorine atoms per photon absorbed, 3.7×10^{15} molecules/cm^3 of ethyl peroxy radicals are generated per Torr of oxalyl chloride. The similar S/N ratio observed in the spectra recorded with the two different methods is consistent with these simple estimates.

3. Results and Analysis

Methyl peroxy (CH_3O_2), as well as ethyl peroxy ($C_2H_5O_2$), possesses only a single isomeric form with a peroxy-like electronic structure. Calculations for methyl peroxy[25] predict one conformer with the stable minimum where the O_2 group is staggered with respect to the methyl H's (the structure with one of the hydrogens eclipsed with the terminal oxygen is a saddle point effectively representing the barrier to the methyl group free rotation). For ethyl peroxy, calculations indicate two stable conformers,[20] T (trans) and G (gauche) versions corresponding to a 0° and 120° (−120°) dihedral angles between the O−O−C and O−C−C planes, respectively. Nonetheless, the spectrum of only one of the two conformers of ethyl peroxy has been previously reported experimentally.[9]

3.1. Overview of Experimental Spectra. Figure 1 shows scans in the 7200−7800 cm^{-1} origin region (Figure 1a), 7650−8250 cm^{-1} COO bend vibrational region (Figure 1b), and 8100−8700 cm^{-1} O−O stretch vibrational region (Figure 1c) for the ethyl peroxy radical. These traces are compared with methyl peroxy radical spectra in the origin[9] and O−O stretch[25] regions. The two ethyl peroxy traces are offset for visualization purposes

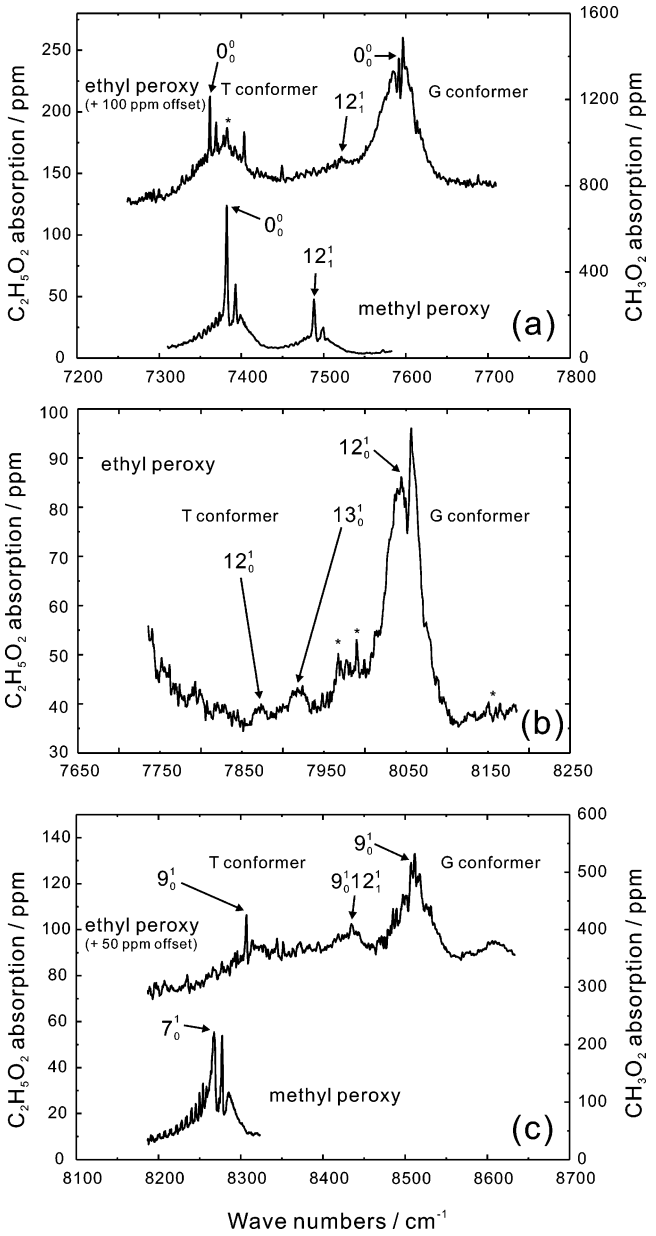

Figure 1. Comparison between the experimental CRDS spectra (digital three-point smoothing was applied) of ethyl peroxy and methyl peroxy radicals in the (a) origin, (b) COO bend vibrational, and (c) O−O stretch vibrational regions. The spectra for ethyl peroxy are manually offset from that of methyl peroxy for a better view in parts a and c. Ethyl peroxy and methyl peroxy radicals are produced following the photolysis of 3-pentanone and acetone, respectively. The origin bands for methyl peroxy and for the T and G conformers of ethyl peroxy are indicated as 0_0^0. The band to higher frequency in the origin region of methyl peroxy arises from a hot methyl torsion transition (12_1^1). The spectrum of the T conformer of ethyl peroxy in the origin region also shows the strong peak of methyl peroxy at 7382 cm^{-1} due to reaction of methyl radicals, produced as a byproduct by the photolysis of 3-pentanone, with O_2 (all bands due to this methyl peroxy byproduct are marked with asterisks, see text for details). The arrows mark the positions of the band centers. Note that in the ethyl peroxy radical, according to Herzberg's notation, the CCO bend vibration is labeled as ν_{13}, the COO bend vibration as ν_{12}, and the O−O stretch vibration as ν_9, whereas the latter one is denoted as ν_7 in methyl peroxy.

by 100 and 50 ppm in parts a and c of Figure 1, respectively. Methyl and ethyl peroxy radicals are produced by the direct photolysis method with acetone and 3-pentanone as precursors, respectively. For the methyl peroxy radical, the band at 7382 cm^{-1} has been assigned to the 0_0^0 origin band of the $\tilde{A}^2A'$-$\tilde{X}^2A''$ transition, whereas the weaker band to higher frequency at 7488 cm^{-1} was attributed to a transition involving the methyl torsion ν_{12} in the radical.[9] The spectrum for ethyl peroxy in the origin region exhibits two prominent features, one around 7360 cm^{-1} and the other in the region of 7600 cm^{-1}, each exhibiting a rather different structural appearance. The stronger, higher frequency feature was assigned to the 0_0^0 origin of the $\tilde{A}^2A'$-$\tilde{X}^2A''$ transition in the ethyl peroxy radical by Pushkarsky et al.[9] They also noticed the weaker absorption band at lower energies and assigned it in part to CH_3O_2 due to its approximate resemblance to the origin band of methyl peroxy. This was consistent, given the then available S/N, with the fact that other CH_3O_2 lines were identified in the spectrum.

All the spectral features shown in Figure 1 disappear completely by increasing the time delay between firing the excimer (i.e., starting the reaction chemistry) and the ringdown probe from 100 μs to 30 ms, which proves that the structure belongs to a transient species and not to stable end-reaction products which might accumulate in the cell. By having a more detailed look at the spectra in Figure 1a, one can identify, as before, the sharp, intense methyl peroxy structure at 7382 cm^{-1} (corresponding mostly to the Q branch) and labeled with an asterisk in Figure 1a. A possible explanation for this peak is that methyl radicals are produced as a byproduct in the photolysis of 3-pentanone. Another contribution to the methyl peroxy signal may come from the self-reaction between ethyl peroxy radicals forming (among other products) acetaldehyde, which itself is a methyl radical precursor upon photolysis. Bands arising from this methyl peroxy byproduct in other parts of the spectrum are also marked with asterisks (see Figure 1b). However, it is clear from the present spectrum that there is additional structure around 7360 cm^{-1}, which is reasonable to assign to the T conformer of the ethyl peroxy radical (see section 3.2 for details).

Because the $\tilde{A}$-$\tilde{X}$ electronic transition is essentially a promotion of an electron to the π^* singly occupied orbital localized on the terminal oxygen, one should expect to observe in the ethyl peroxy spectrum $\tilde{A}$ state vibrations that involve the terminal oxygen atom. Indeed, quite strong $\tilde{A}$ state O−O stretching vibrations of the order of 900 cm^{-1} and COO bend vibrations with moderate intensities of the order of 500 cm^{-1} have been observed for most of the previously investigated alkyl peroxy radicals. Figure 1c shows the O−O stretch region for methyl and ethyl peroxy, and the strong similarities of the absorption contours in the O−O stretch region and origin region for both the methyl and ethyl peroxy spectra give a clear indication that the higher frequency bands can be assigned as the O−O stretch.

Figure 1b depicts the frequency range between the origin and O−O stretch (ν_9, see Table 1) regions, where the COO bend vibration (ν_{12}) is expected. The $\tilde{X}$-$\tilde{A}$ transition to the COO bend vibration in the excited state is easily identified for the G conformer due to its structural similarity to the origin band of the G conformer. For the T conformer only a weak band lacking sharper structure is seen around 7880 cm^{-1}, but this is still in acceptable agreement with the ab initio predicted COO bend vibrational frequency (see section 3.2). Different Franck−Condon factors for the two conformers for the excitation of the COO bend in the $\tilde{A}$ state could explain the smaller intensity ratio between COO bend bands of the T and G conformers compared to the ratios in the origin and O−O stretch regions. This is consistent with Figure 2 (see section 3.2), which shows a significant difference in the $\tilde{A}$-$\tilde{X}$ geometry change for the COO bend.

TABLE 1: Scaled[a] Vibrational Frequencies (in cm^{-1}) Calculated at the EOMIP-CCSD/DZP Level for the Ground and Excited States for the T and G Conformers of $C_2H_5O_2$ and $C_2D_5O_2$

			$C_2H_5O_2$				$C_2D_5O_2$			
			T		G		T		G	
mode	vibrational description	symmetry[b]	$\tilde{X}$	$\tilde{A}$	$\tilde{X}$	$\tilde{A}$	$\tilde{X}$	$\tilde{A}$	$\tilde{X}$	$\tilde{A}$
ν_1	CH str	A′	3109	3112	3108	3118	2304	2306	2304	2313
ν_2	CH_2 sym str	A′	3043	3012	3050	3024	2216	2188	2220	2205
ν_3	CH_3 sym str	A′	3009	3006	3009	3008	2164	2165	2163	2163
ν_4	CH_3 in-plane def	A′	1493	1517	1486	1484	1244	1243	1226	1229
ν_5	CH_2 scissor	A′	1480	1484	1474	1474	1195	1145	1193	1111
ν_6	CH_3 sym def	A′	1422	1423	1413	1418	1066	1065	1071	1071
ν_7	CH_2 wag	A′	1368	1378	1370	1377	1060	1059	1062	1060
ν_8	CH_3 out-of-plane rock	A′	1196	1128	1198	1110	1004	989	997	986
ν_9	O−O str	A′	987	948	951	951	973	935	963	938
ν_{10}	C−C str	A′	1055	1044	1022	994	885	889	856	863
ν_{11}	C−O str	A′	871	873	868	861	714	722	737	735
ν_{12}	COO bend	A′	502	436	526	463	473	402	468	414
ν_{13}	CCO bend	A′	306	285	360	338	274	261	322	304
ν_{14}	CH str	A″	3116	3110	3124	3104	2314	2306	2322	2301
ν_{15}	CH_3 asym str	A″	3097	3060	3102	3099	2299	2276	2301	2299
ν_{16}	CH_3 out-of-plane def	A″	1466	1463	1464	1464	1054	1053	1053	1052
ν_{17}	CH_2 twist	A″	1268	1268	1295	1298	973	977	957	952
ν_{18}	CH_3 in-plane rock	A″	1148	1173	1168	1172	894	908	912	913
ν_{19}	CH_2 rock	A″	797	827	796	797	581	602	591	588
ν_{20}	CH_3 torsion	A″	233	234	238	233	172	170	176	185
ν_{21}	CO torsion	A″	91	138	123	140	87	139	112	119

[a] A scaling factor of 0.97 has been determined from a comparison between the same EOMIP-CCSD/DZP calculations and experimental values for methyl peroxy excluding the OO stretching mode. This scaling factor was applied to all calculated vibrational frequencies except for the O−O stretch mode, which is poorly predicted by these calculations. Therefore, a scaling factor of 0.84 (again determined by a comparison between calculation and experiment for methyl peroxy) was used for the O−O stretch mode, in agreement with the results from our earlier propyl peroxy investigation using EOMIP calculations with a basis set of similar quality.[13] [b] Symmetry label becomes A for the G conformer.

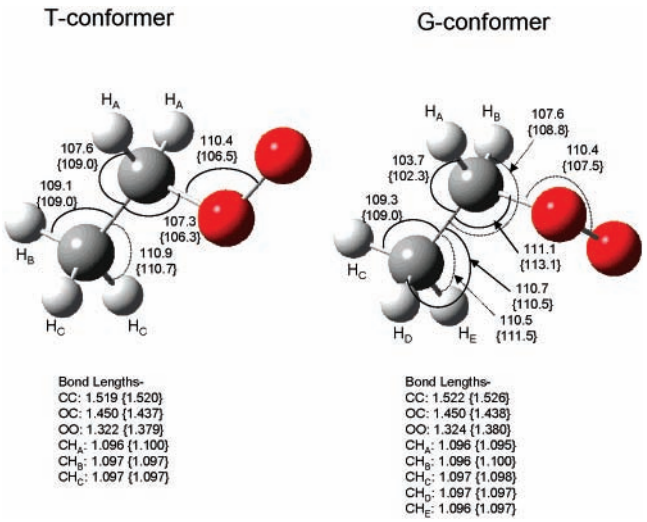

Figure 2. Optimized geometric parameters of the two conformers of the ethyl peroxy radical as obtained at the EOMIP-CCSD/DZP level of theory. The above conformers are labeled as T (trans) or G (gauche) based on their dihedral angle between the O−O−C and O−C−C planes, which is 0° or 120°, respectively. The T conformer has C_s symmetry, and therefore, requires fewer coordinates to describe its geometry than does the G conformer (i.e., two Hs on the CH_2 group and two Hs on the CH_3 group are the same for the T conformer). For both conformers, the bond angles are drawn in on the pictures and labeled in degrees (°) and the bond lengths are listed beneath the pictures in Angstroms (Å). In both cases the first value is for the $\tilde{X}$ state while the second in brackets is for the $\tilde{A}$ state.

In addition, the broad band at 7920 cm^{-1} in Figure 1b was assigned to the CCO bend vibration (ν_{13}) of the G conformer. The assignments of the COO bend vibration of the T and G conformers and the CCO bend vibration of the G conformer were facilitated by comparison with the calculated frequencies (see section 3.2) and have been confirmed by observing the expected isotopic shifts in the spectrum of $C_2D_5O_2$.

3.2. Quantum Chemical Calculations and Experimental Assignments. To support and analyze our spectroscopic observations, we have performed ab initio calculations on the ethyl peroxy radical and its perdeutero analogue. Because we want to assign the $\tilde{A}$-$\tilde{X}$ CRDS spectra of both the T and G conformers of the ethyl peroxy radical, we had to choose computational methods that are capable of handling the ground and excited states of both conformers. The T conformer has C_s symmetry and therefore has different electronic symmetries in the $\tilde{X}$ (A″) and $\tilde{A}$ (A′) states, whereas the G conformer possesses only C_1 symmetry and hence has the same A symmetry in the $\tilde{X}$ and $\tilde{A}$ states. Therefore, we performed equation of motion ionization potential coupled cluster with singles and doubles (EOMIP-CCSD)[26] calculations with the DZP basis set[27] using the corresponding anion as reference. Thereby, the geometries were optimized for both states to determine the adiabatic $\tilde{A}$-$\tilde{X}$ excitation energies. This method turned out to be suitable in our earlier propyl peroxy investigation[13] because this approach treats the ground and excited state in a similar fashion. In addition to the $\tilde{A}$-$\tilde{X}$ excitation energies, the $\tilde{X}$ and $\tilde{A}$ state harmonic vibrational frequencies, as well as the rotational constants for the vibrationless levels of both states, have been calculated with the same method. These EOMIP results were obtained with the ACESII program package.[28] The results from the calculations are shown in Figure 2 and listed in Tables 1 (vibrational frequencies, in the notation of Herzberg[29]) and 2 (rotational constants). The vibrational frequencies shown are scaled by 0.97 from their ab initio values, except for the O−O stretch (see below).

Figure 1a shows the assignment of the two conformers expected for the ethyl peroxy radical. In previous studies of *n*-propyl[13] and *n*-butyl[14] peroxies, both composed of several

TABLE 2: Comparison between the Experimentally Determined and Calculated (EOMIP-CCSD/DZP) Spectroscopic Constants for the T and G Conformers of $C_2H_5O_2$ and $C_2D_5O_2$ for the Origin Transition Frequencies (0_0^0), Conformer Shift of the Origin Frequency between G and T, ν_{12} (COO Bend), ν_{13} (CCO Bend), and ν_9 (O−O Stretch) Vibrational Frequencies, and Rotational Constants *A*, *B*, and *C* in the Ground $\tilde{X}$ (labeled with ″) and Excited $\tilde{A}$ (labeled with ′) State[c]

	experiment				EOMIP calculations			
	$C_2H_5O_2$		$C_2D_5O_2$[a]		$C_2H_5O_2$		$C_2D_5O_2$	
	T	G	T	G	T	G	T	G
0_0^0	7362(1)	7592(1)	7355(1)	7595(1)	7938	8059	7935	8062
$\Delta 0_0^0$ (G-T)	230		240		121		127	
ν_{12} (COO bend)	512	457	483	408	436[b]	463[b]	402[b]	414[b]
ν_{13} (CCO bend)		328		294	285[b]	338[b]	261[b]	304[b]
ν_9 (O−O stretch)	945	915			948[b]	951[b]	935[b]	938[b]
A″	1.107	0.584			1.111	0.589	0.742	0.448
B″	0.148	0.191			0.148	0.189	0.128	0.163
C″	0.138	0.164			0.137	0.163	0.119	0.141
A′	1.087	0.556			1.079	0.554	0.729	0.426
B′	0.149	0.194			0.149	0.194	0.129	0.166
C′	0.138	0.164			0.137	0.163	0.119	0.140

[a] The O−O stretch region was not recorded for $C_2D_5O_2$. Also no rotational contour analysis has been made for this isotope. [b] Scaled EOMIP-CCSD/DZP frequencies (see footnote of Table 1). [c] All values are given in cm^{-1}.

conformers, based upon ab initio calculations the spectral feature observed at the lowest transition frequency was assigned to the T conformer for which the dihedral angle between the O−O−C and O−C−C planes is 0°. Correspondingly, we assign the origin bands at 7361.6 and 7592.0 cm^{-1} in Figure 1a to the T and G conformers of ethyl peroxy, respectively. This is also in agreement with the EOMIP-CCSD/DZP calculations, which predict a lower adiabatic transition frequency for the T than the G conformer. Moreover, these conformer assignments are in agreement with the more conclusive ones resulting from the analysis of the rotational contours (see section 3.4). The EOMIP calculations also predict the T conformer to lie higher in energy than the G one by 81 cm^{-1}. Taking into account a degeneracy factor of 2 and 1 for the G and T conformers, respectively, the equilibrium population at room temperature is therefore decreased by a factor of 3 for the T conformer compared to that of the G conformer, in qualitative agreement with the observed spectrum (see Figure 1a).

The experimental origin transition frequencies for the T and G conformers of ethyl peroxy are listed in Table 2 and are compared with the calculated ones. The absolute calculated values are not in very good agreement with the experimental ones, similar to the results we have seen in the propyl peroxy radical investigation[13] where EOMIP calculations overestimated the absolute values of the $\tilde{A}$-$\tilde{X}$ excitation energies by about 500 cm^{-1}. However, the zero-point energy corrected EOMIP calculations predict a blue shift of the transition frequency of 121 cm^{-1} for the G relative to the T conformer of $C_2H_5O_2$, which is in fairly good agreement with the experimental shift of 230 cm^{-1} (see Table 2). Moreover, the transition frequencies for the T conformers of the linear alkyl peroxies $C_nH_{2n+1}O_2$ investigated so far up to $n = 4$ all lie in the region of 7400 cm^{-1}. We also determined experimental values for the COO bend (ν_{12}) and O−O stretch (ν_9) vibration frequencies for both conformers and the CCO bend (ν_{13}) vibration frequency for the G conformer (see Figure 1b,c and Table 2). (The frequency position of the band assigned to ν_{12} of the T conformer of ethyl peroxy matches also with an overtone transition involving $2\nu_{21}$ in the G conformer, using the calculated vibrational frequencies of Table 1. We can therefore not rule out a possible overlap between these two bands as an assignment of the structure to $2\nu_{21}$. The band is too weak for an investigation of the rotational contour in order to clarify this point in more detail.) For the O−O stretch vibration, the experimental separations from the origin are 945 and 915 cm^{-1} for the T and G conformers, respectively. In our former study[13] on the propyl peroxy radical we have noticed that for the O−O stretching mode the EOMIP-CCSD harmonic vibrational frequencies largely overestimate the experimental values. Therefore we determined a different scale factor for this mode based on the comparison of observed O−O stretching frequencies and EOMIP-CCSD/DZP calculations for methyl peroxy. By using this scale factor (0.84), the O−O stretching frequencies of both conformers are predicted within 1−4% accuracy. The large deviation of the scale factor from unity is a consequence of the anharmonicity of this mode and the fact that the correct quantum chemical description of the O−O bond would require inclusion of higher correlation effects. Since the COO bending mode is coupled with the O−O vibration and we used the scale factor (0.97) determined for modes other than the O−O stretch, the discrepancy between the COO bend scaled value and the experimental observation is somewhat larger than that for the other modes.

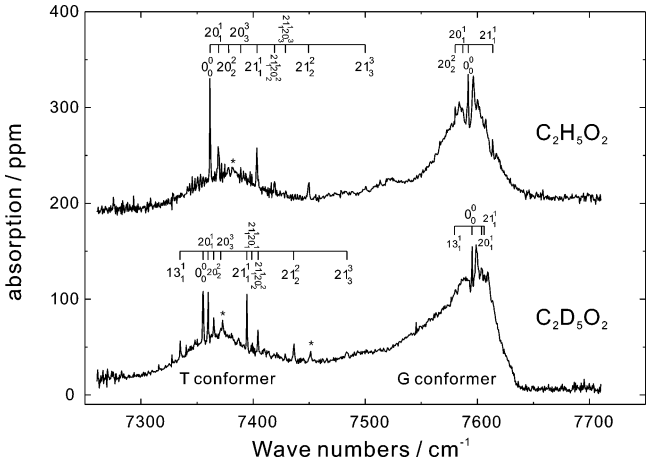

Figure 3. CRDS spectra of the $\tilde{A}^2A'$-$\tilde{X}^2A''$ electronic transition of the ethyl peroxy radical in the origin region taken with ethane (upper trace) and d_6-ethane (lower trace) as precursors and applying the H-abstraction method for peroxy radical generation. The spectrum for $C_2H_5O_2$ is offset by 170 ppm for a better view. Hot bands are labeled according to the $N_{v''}^{v'}$ notation, where v'' and v' are $\tilde{X}$ and $\tilde{A}$ vibrational quantum numbers in vibration N, respectively. The three peaks labeled with an asterisk belong to methyl peroxy and its deuterated analogue, respectively.

TABLE 3: Scaled Frequencies Calculated at the EOMIP-CCSD/DZP Level of the Three Lowest Lying Vibrations in the $\tilde{X}$ Ground State and $\tilde{A}$ First Excited State for the T and G Conformers of Ethyl Peroxy Radical and Its Perdeutero Analogue and a Comparison between the Calculated ($\Delta(\nu_{\tilde{A}} - \nu_{\tilde{X}})$) and Experimental Hot Band Progression Frequencies (relative to the origin)[c]

	calculated			experimental	
	$\tilde{A}$	$\tilde{X}$	$\Delta(\nu_{\tilde{A}} - \nu_{\tilde{X}})$	$\Delta(\nu_{\tilde{A}} - \nu_{\tilde{X}})^a$	$\exp(-\nu_{\tilde{X}}/kT)^b$
T conformer	138	91	47	42(1)	0.64
of $C_2H_5O_2$	234	233	1	8(1)	0.32
	285	306	−21	not observed	0.23
T conformer	139	87	52	39(1)	0.66
of $C_2D_5O_2$	170	172	−2	4(1)	0.44
	261	274	−13	−21(1)	0.27
G conformer	140	123	17	22(1)	0.55
of $C_2H_5O_2$	233	238	−5	−5(1)	0.32
	338	360	−22	not observed	0.18
G conformer	119	112	7	11(1)	0.58
of $C_2D_5O_2$	185	176	9	8(1)	0.43
	304	322	−18	−16(1)	0.21

[a] Experimental values are obtained by measuring the separation between the 0_0^0 band and the first member of the hot band progression according to the assignment in Figure 3. [b] Level population at room temperature of the three lowest lying vibrations relative to the vibrationless level. The next lowest vibrational frequencies for both conformers and isotopes are >450 cm^{-1} with a corresponding level population of <0.12 relative to the vibrationless level, and were therefore not considered in the analysis. The degeneracy factors of 1 and 2 for the T and G conformers, respectively, and the difference between the absolute energies of the T and G conformers are not reflected in these values (see text for details). [c] The corresponding population of these vibrations in the ground state relative to the vibrationless state is listed in the last column. All frequency values are in cm^{-1}.

3.3. Sequence Band Structure. Figure 3 shows a comparison between the spectra of normal ethyl peroxy (upper trace) and its fully deuterated analogue (lower trace) in the origin region. The observed red shift of 7 cm^{-1} and blue shift of 3 cm^{-1} upon deuteration for the origin transitions of the T and G conformers of ethyl peroxy, respectively, is explainable because of the change in the zero-point energy levels. Our EOMIP calculations predict a difference between $\tilde{A}$ and $\tilde{X}$ zero-point energies for the protonated and deuterated T ethyl peroxy of −74 and −77 cm^{-1}, respectively, leading to a calculated red shift of 3 cm^{-1}, in very good agreement with the experiment. For the G conformer, the same considerations predict a blue shift of 3 cm^{-1}, in quantitative agreement with the experimental observation.

With the help of the above-mentioned vibrational frequency calculations (given in Table 1), the general appearance of the spectra in Figure 3 for the T conformer can be explained by the presence of vibrational hot bands. Transitions from thermally populated vibrational levels in the $\tilde{X}$ state to the vibrational levels of the same symmetry in the $\tilde{A}$ state are allowed and similar observations were made in the study of acetyl peroxy by Miller and co-workers.[11] Table 3 gives frequencies for the three lowest lying vibrational modes in the $\tilde{A}$ and $\tilde{X}$ states. According to the table, excitations to the $\tilde{A}$ state in the T conformer of $C_2H_5O_2$ will result in an increase of the CO torsion (ν_{21}) and a decrease of the CCO bend (ν_{13}) vibrational frequencies, whereas the CH_3 torsional motion (ν_{20}) is nearly unaffected. Therefore a blue-shifted (positive values in the fourth column of Table 3) CO torsional and a red-shifted (negative values) CCO bend progression are expected in the spectrum, which is in good agreement with what is observed (see Figure 3). The CH_3 torsional motion appears as a slightly blue-shifted progression in the spectrum. Table 3 compares the calculated and experimental frequencies for these progressions in the fourth and fifth columns. Overall, we have assigned several members of the CO and CH_3 torsion hot band progressions in addition to the first member of the CCO bend hot band progression and two hot bands originating from ν_{21} and ν_{20} combination bands, whose intensities, as expected, are quite weak. Positions of the hot bands and shifts relative to the origin are presented in Table 4 and depicted in Figure 3 for the two conformers of $C_2H_5O_2$ and $C_2D_5O_2$. In particular, we have observed for the T conformer of the ethyl peroxy two blue-shifted progressions of 42 and 8 cm^{-1} spacings (separation between the 0_0^0 band and first member of the hot band progression), in reasonable agreement with the ab initio predictions, and therefore they have been assigned to the CO and methyl torsion progressions, respectively. Figure 3 clearly shows that the CH_3 torsion (ν_{20}) hot band progression exhibits smaller separations between its members in going from the normal to the deuterated ethyl peroxy radical, whereas the CO torsion (ν_{21}) is almost unaffected by deuteration, leaving the separations in the ν_{21} hot band progression nearly unchanged. The calculations even predict a change from a small blue to a slightly red-shifted CH_3 torsion progression upon deuteration. In addition, we also observe the first member of the CCO bend progression in the deuterated ethyl peroxy T conformer. The frequency of the CCO bend vibration in the ground state is smaller for the deuterated species than the one for the normal ethyl peroxy radical, leading to a small increase of the level population relative to the origin band for $C_2D_5O_2$ (see the last column of Table 3). This together with the slightly more pronounced and dense rotational contour to the red of the origin band in $C_2H_5O_2$ makes the hot band progression involving ν_{13} observable for $C_2D_5O_2$ but not for $C_2H_5O_2$. The possibility of assigning any of the observed structure in this region to $\tilde{X}$ vibrational overtones of which the strongest transitions would mostly involve at least one, and more likely two quanta of CH stretch can be ruled out because the deuteration effect of such overtones would have been much more pronounced, contradictory to the experimental observation.

For the G conformer of ethyl peroxy the calculations predict a red-shifted hot band progression involving CH_3 torsion for $C_2H_5O_2$, which changes to a blue-shifted one upon deuteration. In addition, also the CO torsion hot band progression is affected by going from $C_2H_5O_2$ to $C_2D_5O_2$ in the G conformer. With the help of the calculations given in Table 3, we could assign hot band progressions involving the CO and methyl torsion in both isotopes as well as the hot band progression involving the CCO bend in $C_2D_5O_2$. Not all peaks observed in Figure 3 belong to vibrational hot bands, because, especially for the G conformer, the rotational envelope overlaps with them (see section 3.4). The agreement between predicted and measured shifts of all these hot band progressions in $C_2H_5O_2$ and $C_2D_5O_2$ is quite good, as can be seen in Table 3. Table 4 summarizes the origin frequencies and hot band positions observed for both conformers T and G of the normal and deuterated ethyl peroxy.

3.4. Rotational Structure. The reason why the hot band progressions are more expressed and visible for the T than the G conformer (see Figure 3) lies in the fact that the two conformers exhibit different rotational contours due to their different symmetries. In the T conformer with C_s symmetry the $\tilde{A}^2A'$-$\tilde{X}^2A''$ transition possesses a pure *c*-type transition moment, whereas in the G conformer with C_1 symmetry, the $\tilde{A}^2A$-$\tilde{X}^2A$ transition is a mixture of *a*-, *b*-, and *c*-type transition moments. The traces in Figure 4a show on an expanded scale a portion of the ethyl peroxy spectrum in the origin region for the T and G

TABLE 4: Observed Origin Frequencies, Hot Band Positions, and Their Relative Shifts with Respect to the Origin for Both T and G Conformers of $C_2H_5O_2$ and $C_2D_5O_2$[c]

		T conformer		G conformer	
	assignment[a]	position[b]	$\Delta(\nu_{hotband}-0_0^0)$	position[b]	$\Delta(\nu_{hotband}-0_0^0)$
$C_2H_5O_2$	0_0^0	7361.6	0	7592.0	0
	21_1^1	7403.5	41.9	7613.8	21.8
	21_2^2	7449.4	87.8		
	21_3^3	7500.1	138.5		
	20_1^1	7369.3	7.7	7587.1	−4.9
	20_2^2	7378.1	16.5	7580.3	−11.7
	20_3^3	7389.0	27.4		
	$21_1^1\,20_2^2$	7419.2	57.6		
	$21_1^1\,20_3^3$	7428.8	67.2		
$C_2D_5O_2$	0_0^0	7355.4	0	7595.3	0
	21_1^1	7394.4	39.0	7606.1	10.8
	21_2^2	7436.1	80.7		
	21_3^3	7483.7	128.3		
	20_1^1	7359.8	4.4	7603.7	8.4
	20_2^2	7364.8	9.4		
	20_3^3	7371.1	15.7		
	13_1^1	7334.2	−21.2	7579.7	−15.6
	$21_1^1\,20_1^1$	7398.9	43.5		
	$21_1^1\,20_2^2$	7404.5	49.1		

[a] The levels are labeled according to the $N_{v''}^{v'}$ notation, where v'' and v' are $\tilde{X}$ and $\tilde{A}$ vibrational quantum numbers in vibration N, respectively. Vibration ν_{21} is the CO torsion, ν_{20} the methyl torsion, and ν_{13} the CCO bend. [b] The accuracy of the calibration procedure (comparison of the frequencies of residual water lines with HITRAN database) is better than 0.5 cm^{-1}, but because of different rotational contours, the precision of the resulting vibrational frequencies is estimated to be about 1 cm^{-1}, which corresponds to an average value of the fwhm of the peaks. [c] All values are in cm^{-1}.

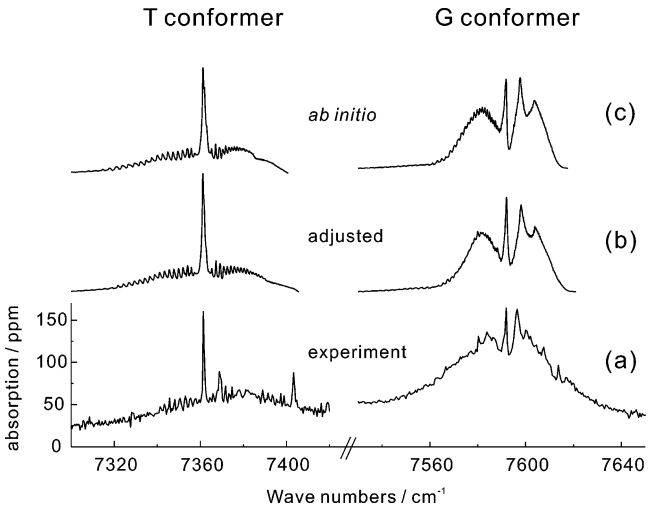

Figure 4. Spectra of the T and G conformers of $C_2H_5O_2$ radical from (a) the CRDS experiment, (c) a simulation using ab initio rotational constants, and (b) a simulation designed to best reproduce the experimental spectrum by adjusting the ab initio rotational constants to best fit values. The best fit and the ab initio values used are given in Table 2. The simulations for the T conformer used a pure *c*-type transition moment whereas in those for the G conformer, the ratio of the components of the transition dipole along the inertial axes is *a*:*b*:*c* = 8:6:5, taken to best reproduce the observed spectrum.

conformers. The individual peaks correspond to the rotational contours of vibronic transitions. Room temperature simulations of the rotational contour for the observed $\tilde{A}^2A'$-$\tilde{X}^2A''$ transition were generated by our SpecView analysis [V. L. Stakhursky, http://molspect.mps.ohio-state.edu/goes/specview.html] using purely ab initio rotational constants (see Table 2) and are shown in Figure 4c. The simulations neglect any spin-rotation effects due to the doublet nature of the electronic state. As parts a and c of Figure 4 show, there is already a good resemblance between the experimental spectra and the ones predicted by the ab initio constants. By slightly adjusting the ab initio rotational constants of both the $\tilde{X}$ and $\tilde{A}$ states, an even better match with the experimental spectrum can be achieved. Because the rotational envelopes for the T and G conformers of the ethyl peroxy are so different, the good agreement between the simulations and the observed spectra confirms that the bands have been correctly assigned to the T and G conformers, independent of the previous argument based upon the calculated shifts in the transition frequencies.

The values of the rotational constants relative to each other in the ground and excited state have a sensitive effect on the observed rotational contours. Simulations at our resolution for the T conformer of ethyl peroxy, in which for instance B'' and C'' have been decreased by only 8% and 5%, respectively, and leaving all the other constants fixed, resulted in rotational contours where the intense, sharp peak consisting mostly of Q branch transitions is spread out over the whole rotational contour, resulting in only a broad band. (This effect could explain the fact that no intense sharp peak has been observed for the T conformer in the COO bend vibrational band (see Figure 1).) The values of the adjusted and ab initio rotational constants used in Figure 4b,c are summarized in Table 2. The features observed in the T conformer (Figure 4a) but which do not show up in the simulations (Figure 4b,c) arise from hot band progressions (see section 3.3). A convolution of individual rotational contours of the origin band and multiple vibrational hot bands gives rise to the spectra shown in Figures 1 and 3.

3.5. Absorption Cross Section. Although the spectral analysis is the main purpose of this paper, we have also attempted to estimate the peak absorption cross section σ_p for the $\tilde{A}$-$\tilde{X}$ $C_2H_5O_2$ transition under our experimental conditions. This is straightforward from the standard relationship[30] for the fractional absorption of light of intensity, $\Delta I_p/I_0$,

$$\Delta I_p/I_0 = N\sigma_p l \qquad (1)$$

as long as the concentration, N, is known since l, the length of the sample, is measured to be 13 cm.

N can be estimated from the measurement of the absorption of excimer photolysis photons with and without $(COCl)_2$ in the cell and its known cross section.[24,31] Assuming room temperature equilibrium and the calculated energy gap between the T and G conformers we deduce N for the G conformer to be 1.9×10^{15} molecules/cm^3 when $(\Delta I_p/I_0) = 107$ ppm. This results in a $\sigma_p = 0.44 \times 10^{-20}$ cm^2/molecule for G $C_2H_5O_2$ whereas a value of $\sigma_p = 0.30(15) \times 10^{-20}$ cm^2/molecule has been previously reported.[18] This can be compared to a value of 2.7×10^{-20} cm^2/molecule reported[9] for CH_3O_2 under similar conditions, but using a different approach to measure N.

Part of this sizable difference results from different rotational contours. We estimated this rotational factor, R, by simulating with our SpecView program[32] the spectrum of CH_3O_2 and $C_2H_5O_2$, which in each case is in very good agreement with the observed spectrum. We normalize the peak intensities by the respective integrated spectrum. R is defined by

$$R = \left(\frac{\text{integrated absorption}}{\text{peak absorption}}\right)_{C_2H_5O_2} \times \left(\frac{\text{peak absorption}}{\text{integrated absorption}}\right)_{CH_3O_2} \quad (2)$$

where the subscripts denote the corresponding quantity for the indicated molecule. We find $R = 1.32$ for the G conformer and 0.80 for the T conformer of $C_2H_5O_2$.

This rotational structure factor is a non-negligible part of the observed difference in σ_p for CH_3O_2 and $C_2H_5O_2$. However, even taking this into account, it appears that the intrinsic oscillator strength proportional to $R\sigma_p$ of G $C_2H_5O_2$ is still almost 5 times smaller than that for the methyl peroxy. More precise experiments are warranted to determine how reliable this estimated difference is.

4. Conclusions

The NIR $\tilde{A}^2A'$-$\tilde{X}^2A''$ electronic transition of ethyl peroxy radical and its deuterated analogue has been studied by CRDS. For the first time spectra of both conformers, T and G, have been conclusively observed and assigned. An analysis of the partially resolved rotational structures confirmed the conformer assignments. EOMIP-CCSD/DZP calculations have been carried out to help assign the observed spectroscopic features involving vibrational hot bands, COO bend, and O−O stretch fundamentals in the $\tilde{A}$ state and the rotational contours. The observed $C_2H_5O_2$ origin band lies at 7362(1) cm^{-1} for the T and 7592(1) cm^{-1} for the G conformer, respectively. The shift between the origin transition frequencies for these two conformers is in good agreement with the ab initio calculations. Moreover, the results obtained in this work fit well into trends derived from the earlier investigations of other alkyl peroxy radicals, which will be the topic of an upcoming paper.[16]

Two methods of ethyl peroxy radical production were used, direct photolysis of 3-pentanone and hydrogen abstraction from ethane by Cl atoms following the photolysis of oxalyl chloride to produce ethyl radicals which then subsequently reacted with O_2 to generate the peroxy radicals. Both methods resulted in spectra with good S/N ratios and provided independent proof of the spectral carrier. The present results can be used to follow the dynamics and reactions of ethyl peroxy radicals in a conformer-specific manner. Moreover, a high-resolution solid-state laser system combined with a cavity ringdown spectrometer involving a discharge slit-jet expansion was recently developed in our group[33] and will allow us, based upon the results of this work, to perform detailed rotational analysis of small peroxy radicals like methyl and ethyl peroxy, using as a foundation this and previous analyses of the room temperature spectra.

Acknowledgment. We wish to acknowledge the financial support of this work by the Chemical Sciences, Geosciences and Biosciences Division, Office of Basic Energy Sciences, Office of Science, U.S. Department of Energy, via grant DE-FG02-01ER15172. P.R. thanks the Swiss National Science Foundation for a postdoctoral fellowship. G.T. acknowledges the support of the Zoltán Magyary Foundation and the Hungarian Scientific Research Fund (OTKA F049722).

References and Notes

(1) Robertson, S. H.; Seakins, P. W.; Pilling, M. J. In *Low-temperature combustion and autoignition*; Elsevier: Amsterdam, The Netherlands, 1997; Vol. 35, Chapter 2.

(2) Kee, R. J.; Coltrin, M. E.; Glarborg, P. In *Chemically Reacting Flow*: *Theory and Practice*; Wiley-Interscience: New York, 2003.

(3) D'Anna, A.; Violi, A.; D'Alessio, A. *Combust. Flame* **2000**, *121*, 418.

(4) Lightfoot, P. D.; Cox, R. A.; Crowley, J. N.; Destriau, M.; Hayman, G. D.; Jenkin, M. E.; Moortgat, G. K.; Zabel, F. *Atmos. Environ.* **1992**, *26A*, 1805.

(5) Orlando, J. J.; Tyndall, G. S.; Wallington, T. J. *Chem. Rev.* **2003**, *103*, 4657.

(6) Wallington, T. J.; Dagaut, P.; Kurylo, M. J. *Chem. Rev.* **1992**, *92*, 667.

(7) Wallington, T. J.; Nielsen, O. J. In *Peroxyl Radicals*; John Wiley and Sons: New York, 1997; p 457.

(8) Jafri, J. A.; Phillips, D. H. *J. Am. Chem. Soc.* **1990**, *112*, 2586.

(9) Pushkarsky, M. B.; Zalyubovsky, S. J.; Miller, T. A. *J. Chem. Phys.* **2000**, *112*, 10695.

(10) Zalyubovsky, S. J.; Wang, D.; Miller, T. A. *Chem. Phys. Lett.* **2001**, *335*, 298.

(11) Zalyubovsky, S. J.; Glover, B. G.; Miller, T. A. *J. Phys. Chem. A* **2003**, *107*, 7704.

(12) Zalyubovsky, S. J.; Glover, B. G.; Miller, T. A.; Hayes, C.; Merle, J. K.; Hadad, C. M. *J. Phys. Chem. A* **2005**, *109*, 1308.

(13) Tarczay, G.; Zalyubovsky, S. J.; Miller, T. A. *Chem. Phys. Lett.* **2005**, *406*, 81.

(14) Glover, B. G.; Miller, T. A. *J. Phys. Chem. A* **2005**, *109*, 11191.

(15) Just, G. M. P.; Sharp, E. N.; Zalyubovsky, S. J.; Miller, T. A. *Chem. Phys. Lett.* **2006**, *417*, 378.

(16) Sharp, E. N.; Rupper, P.; Miller, T. A. In preparation.

(17) Hunziker, H. E.; Wendt, H. R. *J. Chem. Phys.* **1976**, *64*, 3488.

(18) Atkinson, D. B.; Spillman, J. L. *J. Phys. Chem. A* **2002**, *106*, 8891.

(19) Mah, D. A.; Cabrera, J.; Nation, H.; Ramos, M.; Sharma, S.; Nickolaisen, S. L. *J. Phys. Chem. A* **2003**, *107*, 4354.

(20) Rienstra-Kiracofe, J. C.; Allen, W. D.; Schaefer, H. F., III *J. Phys. Chem. A* **2000**, *104*, 9823.

(21) Rothman, L. S.; Jacquemart, D.; Barbe, A.; Benner, D. C.; Birk, M.; Brown, L. R.; Carleer, M. R.; Chackerian, C., Jr.; Chance, K.; Coudert, L. H.; Dana, V.; Devi, V. M.; Flaud, J.-M.; Gamache, R. R.; Goldman, A.; Hartmann, J.-M.; Jucks, K. W.; Maki, A. G.; Mandin, J.-Y.; Massie, S. T.; Orphal, J.; Perrin, A.; Rinsland, C. P.; Smith, M. A. H.; Tennyson, J.; Tolchenov, R. N.; Toth, R. A.; Vander Auwera J.; Varanasi, P.; Wagner, G. *J. Quant. Spectrosc. Radiat. Transfer* **2005**, *96*, 139.

(22) Ito, H.; Nogata, Y.; Matsuzaki, S.; Kuboyama, A. *Bull. Chem. Soc. Jpn.* **1969**, *42*, 2453.

(23) Giuliani, A.; Motte-Tollet, F.; Delwiche, J.; Mason, N. J.; Jones, N. C.; Gingell, J. M.; Walker, I. C.; Hubin-Franskin, M.-J. *J. Chem. Phys.* **2000**, *112*, 6285.

(24) Baklanov, A. V.; Krasnoperov, L. N. *J. Phys. Chem. A* **2001**, *105*, 97.

(25) Zalyubovsky, S. J. Ph.D. Thesis, The Ohio State University, Columbus, Ohio, 2004.

(26) Stanton, J. F.; Gauss, J. *J. Chem. Phys.* **1994**, *101*, 8938.

(27) Dunning, T. H.; Hay, P. J. In *Methods of Electronic Structure Theory*; Plenum Press: New York, 1977; Vol. 2.

(28) Stanton, J. F.; Gauss, J.; Lauderdale, W. J.; Watts, J. D.; Bartlett, R. J. ACESII. The package also contains modified versions of the Molecule GAUSSIAN integral program of J. Almlöf and P. R. Taylor, the ABACUS integral derivative program written by T. U. Helgaker, H. J. Aa. Jensen, P.

Jörgensen, P. R. Taylor, and the PROPS property evaluation integral code of P. R. Taylor.

(29) Herzberg, G. *Molecular Spectra and Molecular Structure*; Infrared and Raman Spectra of Polyatomic Molecules, Vol. II; Krieger Publishing: Malabar, 1991.

(30) Bernath, P. *Spectra of Atoms and Molecules*; Oxford University Press: New York, 1995.

(31) Ahmed, M.; Blunt, D.; Chen, D.; Suits, A. G. *J. Chem. Phys.* **1997**, *106*, 7617.

(32) Stakhursky, V. L.; Miller, T. A. 56th OSU International Symposium on Molecular Spectroscopy, Columbus, OH, June 11−15, 2001 (unpublished).

(33) Wu, S.; Dupré, P.; Miller, T. A. *Phys. Chem. Chem. Phys.* **2006**, *8*, 1682.